JACS
JOURNAL OF THE AMERICAN CHEMICAL SOCIETY

Communication

pubs.acs.org/JACS

Long-Range Ordering of Highly Charged Self-Assembled Nanofilaments

Liam C. Palmer,[†,⊥] Cheuk-Yui Leung,[‡,⊥] Sumit Kewalramani,[§,⊥] Rohan Kumthekar,[†] Christina J. Newcomb,[§] Monica Olvera de la Cruz,[†,‡,§] Michael J. Bedzyk,*[,‡,§] and Samuel I. Stupp*[,†,§,∥]

[†]Departments of Chemistry, [‡]Physics and Astronomy, and [§]Materials Science and Engineering, Northwestern University, Evanston, Illinois 60208, United States

[∥]Department of Medicine and Simpson Querrey Institute for BioNanotechnology, Northwestern University, Chicago, Illinois 60611, United States

Supporting Information

ABSTRACT: Charged nanoscale filaments are well-known in natural systems such as filamentous viruses and the cellular cytoskeleton. The unique properties of these structures have inspired the design of self-assembled nanofibers for applications in regenerative medicine, drug delivery, and catalysis, among others. We report here on an amphiphile of completely different chemistry based on azobenzene and a quaternary ammonium bromide headgroup that self-assembles into highly charged nanofibers in water and orders into two-dimensional crystals. Interestingly small-angle X-ray scattering (SAXS) shows that these fibers of 5.6 nm cross-sectional diameter order into crystalline arrays with remarkably large interfiber spacings of up to 130 nm. Solution concentration and temperature can be adjusted to control the interfiber spacings, and addition of salt destroyed the crystal packing indicating the electrostatic repulsions are necessary for the observed ordering. Our findings here demonstrate the universal nature of this phenomenon in systems of highly charged nanoscale filaments.

Networks of one-dimensional (1D) cytoskeletal components such as actin and microtubules are essential to mediate important biological processes like cell division, protein transport, and signaling.[1,2] Self-assembled nanofibers[3] have also attracted attention for their ability to mimic the extracellular matrix and promote tissue regeneration. Recently, a pathway was discovered to create monodomain hydrogels of peptide amphiphile nanofibers that can align and guide cell migration.[4,5] These monodomain gels could also have anisotropic mechanical and transport properties. Furthermore, it may be possible to use aligned 1D nanostructures as templates for inorganic semiconductor materials as pathways to move charge carriers in transistors or photovoltaic devices.[6] Advancing these important applications will require a deeper understanding of the fundamental mechanisms and pathways to orient 1D objects.[7]

It is known from filamentous viruses[8−10] and self-assembling cyclic peptides[11] that like-charged nanofibers can form crystalline bundles with wall-to-wall separation on the order of their diameters. Counterintuitively, the crystallization of these structures into bundles is driven by fluctuation-induced attractive interactions between neighboring nanofibers.[12,13] Added salts, particularly divalent cations, can also induce crystallization by bridging adjacent fibers through exponentially decaying attractive forces.[9,14] In contrast to the filament bundling driven by attractive forces, a recent study of peptide amphiphile nanofibers at ∼20 mM concentration showed the formation of a fibrillar network driven by *repulsions* between the negatively charged fibers using small-angle X-ray scattering (SAXS).[15] Interestingly, X-ray irradiation was found to create additional charges on the surface of these fibers, causing bundle formation at even lower concentrations (5−10 mM). It was proposed that the long nanofibers formed at the early stages of self-assembly create a stable network, which templates the elongation of short nanofibers within the growing bundle. The repulsion between these highly charged nanofibers is balanced by spatial confinement imposed by neighboring bundles within the network.

Inspired by the anisotropic hexagonal packing of nanostructures observed for peptide amphiphile nanofibers, we designed amphiphilic molecules with a permanent charge (nonionizable) in the headgroup based on aromatic groups in place of the hydrogen-bonding peptides. In water, these molecules self-assemble into 1D nanofibers that are expected to have a very high surface charge density. It has been previously argued that if the fibers form networks, the strong electrostatic repulsion between the confined fibers leads to highly spaced fibers arranged into a 2D hexagonal crystal.[15,16] We investigate here the ability of the fibers to form networks driven by electrostatic repulsion at low concentration (2−16 mM). These networks are studied by solution SAXS as a function of concentration and temperature.

The amphiphilic molecule studied here (**1**) is based on an aromatic azobenzene group, with a hydrophobic tail of ten carbons, and a permanent +1 charged headgroup (see Figure 1a for molecular structure). The synthesis of this molecule with a Br^- counterion is described in detail in the Supporting Information. In water, these molecules dissolve to form viscous, yellow-orange solutions that are birefringent at or above 8 mM (see Figures S2 and S3). Cryogenic transmission electron microscopy (TEM) shows formation of high aspect ratio

Received: August 11, 2014
Published: September 25, 2014

   dx.doi.org/10.1021/ja5082519 | J. Am. Chem. Soc. 2014, 136, 14377−14380

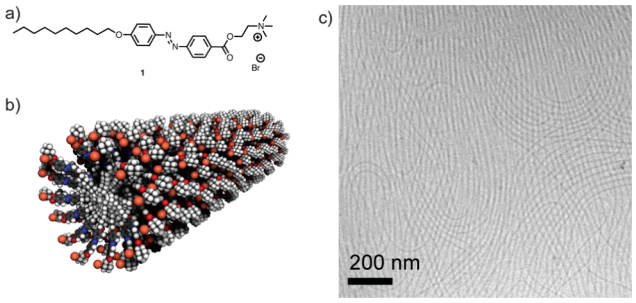

Figure 1. (a) Molecular structure of amphiphile **1** and schematic representation of self-assembled nanofiber. (b) Representative cryogenic TEM images of nanofibers formed by self-assembly of cation **1** (1 mM in water).

nanofibers in aqueous solution (Figure 1c). Despite the strong electrostatic repulsions between the charged headgroups, the self-assembled 1D nanostructure is likely stabilized by attractions, such as van der Waals and $\pi-\pi$ stacking interactions or electrostatic screening by condensed Br^- counterions. Azobenzene amphiphiles in their *trans* form are known to self-assemble[17] and form liquid-crystalline phases[18] at higher concentration, suggesting that excluded volume interactions characteristic of liquid crystals may also promote anisotropy within a dense medium of nanofibers. Photoisomerization to the *cis* configuration was not observed for these molecules when assembled in water, suggesting that they are tightly packed within the nanofiber structure.

We used solution-phase SAXS[19] to explore how these self-assembled nanofibers ordered from 2 to 16 mM in water. The processed SAXS data are shown in Figure 2a as a function of the scattering vector q. For 4−16 mM solutions, the scattered intensity profiles show sharp diffraction peaks in the 0.1−0.5 nm^{-1} q-range indicating long-range ordering in the assembly of nanofibers. The positions of the peaks follow q/q^* ratios of $1:\sqrt{3}:2:\sqrt{7}:3:\sqrt{12}$ (where q^* is the principal peak position), corresponding to 2D hexagonal lattices. The center-to-center spacing [lattice constant (l)] between the nanofibers varies from l = 63 nm for c = 16 mM solution to l = 128 nm for c = 4 mM solution, in accordance with $l \propto c^{-1/2}$ (Figure 2b). The exponent 1/2 is expected for a lattice of 1D objects that is expanding in two dimensions. The domain size of the 2D lattice can be estimated by the Scherrer equation to be on the order of 1 μm. The SAXS data also provide insights into the nanofiber dimensions. Because the lattice is hexagonal, the lattice parameter is related to the volume fraction (V_f) of **1** in solution via

$$l = \sqrt{\frac{2\pi}{3V_f}}\, r \qquad (1)$$

where r is the radius of the nanofilament. Using the solid-state density of 1.28 g/mL measured by gas pycnometry, the known mass of the amphiphile in the solution and eq 1, we estimate a nanofiber radius of 2.8 nm (Figure 1c), which is slightly less than the fully extended molecular length of 3.1 nm, estimated by molecular modeling. These observations imply that for 16 mM solutions, the interfiber spacing is ∼11 times greater than the fiber diameter. In contrast to nanofiber radius, the scattered intensity profile is not very sensitive to the persistence length L of the nanofibers (Figures S4 and S6). At present, we can only place a lower limit of L = 30 nm on the nanofiber persistence length. (Figure S4 and accompanying text).

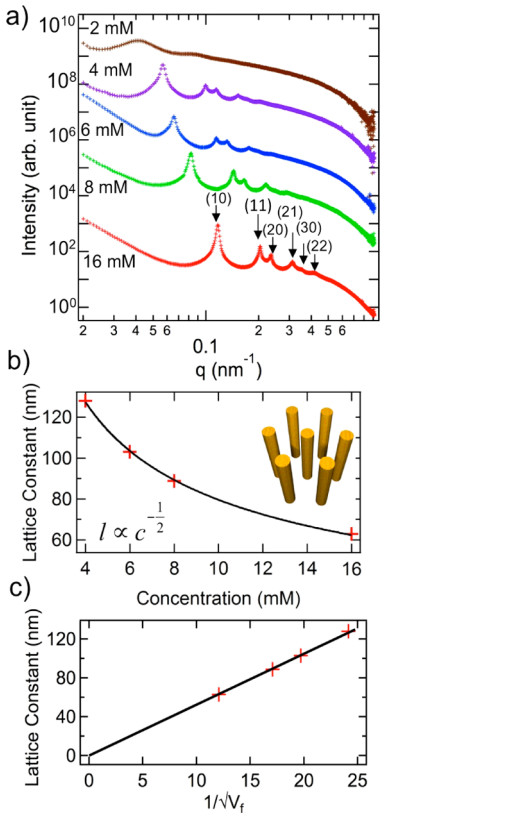

Figure 2. (a) *In situ* SAXS data showing the background subtracted scattered intensity versus the scattering vector q (log−log plot) for amphiphile **1** in water as the solution is diluted from 16 to 2 mM. The data sets are offset vertically for clarity. (b) The lattice constant of the hexagonal lattice formed by the nanofibers versus the solution concentration. (c) The variation of lattice constant with the volume fraction (V_f) of amphiphile.

To understand the origin of the nanofiber packing, we use the nanofiber radius and bulk density of amphiphile **1** to estimate a surface charge density of about 0.22 C/m^2 (which corresponds to about +34e/nm). Charged filamentous viruses, like tobacco mosaic virus (TMV), are known to pack with liquid-like order in solution with a center-to-center spacing on the order of 60 nm.[20] The diameter of TMV is ∼18 nm, and the magnitude of the surface charge density of TMV rods was reported to be 0.04 C/m^2,[21] much lower than the value for our nanofiber system. In that system, the lower linear charge density for TMV results in a much smaller ratio of interfiber separation to the particle diameter. Although the condensation of bromide counterions may reduce the actual charge density in our system,[22] we expect the system is still highly charged. Addition of even 2 mM NaCl or 1 mM $CaCl_2$ or $MgCl_2$ screens the repulsion, and the hexagonal packing disappears (Figure S5 and S6). We conclude that the high linear charge density contributes to strong repulsion among the nanofibers, enabling formation of the observed hexagonally packed network with exceptionally large d-spacings.

As we lower the concentration (c) of amphiphile **1** below 4 mM, the sharp diffraction peaks are replaced by broad intensity modulations, indicating only short-range correlations among the nanofibers at 2 mM (Figure 2a). It is worth noting that the nanofiber morphology is maintained even at these low concentrations (Figure 1c). The differences between high and low concentrations can be more clearly seen in the radial

dx.doi.org/10.1021/ja5082519 | J. Am. Chem. Soc. 2014, 136, 14377−14380

distribution function (RDF) $g(r)$ (Figure S7 and accompanying text), which is a measure of the number density of nanofibers as a function of radial distance from any given nanofiber.[23] The first maximum of the RDF for the 2 mM solution (Figure S7a) gives the nearest-neighbor distance of ~150 nm. The very broad second maximum in $g(r)$ coupled with the rapid decay of $g(r)$ indicates the loss of crystalline ordering. In contrast, for a more concentrated sample with long-range order, sharp peaks show up in the RDF (Figure S7c), and the amplitude of the peaks remains strong over many oscillations. These results indicate that above 2 mM the nanofibers are ordered in a crystalline lattice; at lower concentrations, only short-range correlations between the fibers are observed. The results of sample dilution show that it is possible to control the ordering and interfiber distances by varying concentration.

We examined the solutions as a function of temperature to understand the thermal stability of the system. Changes in the packing behavior were observed by heating a 16 mM solution from 20 to 90 °C (see Figure 3a). From 20 to 40 °C, the

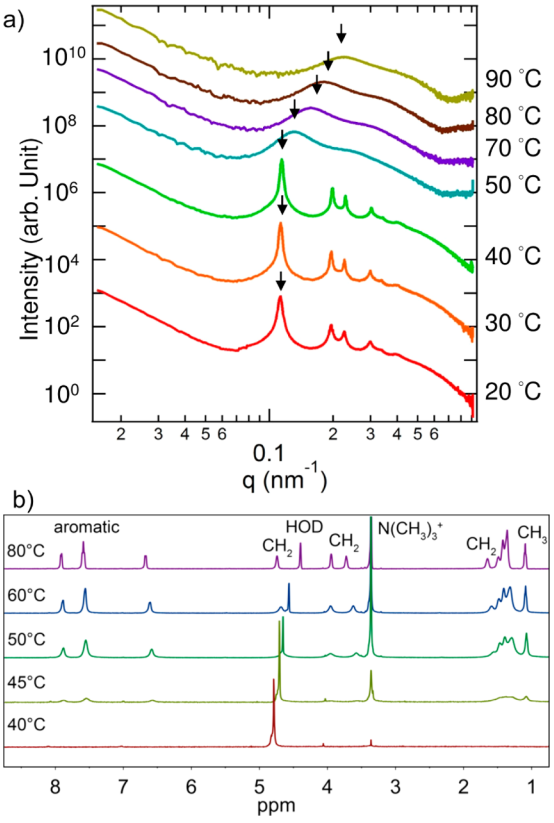

Figure 3. (a) SAXS data showing the background subtracted scattered intensity versus the scattering vector q (log–log plot) for amphiphile **1** in water as the solution temperature changes from 20 to 90 °C. The data sets are offset vertically for clarity. (b) Variable-temperature ^{1}H NMR of 16 mM amphiphile **1** in D_2O shows a transition at 50 °C.

hexagonal peak positions remain constant, i.e., the lattice parameter is unchanged. When the temperature is increased to 50 °C, the hexagonal packing transforms into liquid-like ordering of nanofibers, as indicated by the broad peaks in the SAXS data. As we heat the solution further, this correlation peak position shifts to higher q, which indicates a reduction in the average spacing between the nanofibers. For samples heated up to 70 °C, the change is reversible, and the hexagonal packing is restored upon cooling. In contrast, if these nanofiber solutions are heated to 80 °C or higher, they maintain their liquid-like order upon cooling, indicating an irreversible change in the network structure. However, the similarity between the SAXS intensity profiles at 50 and 80 °C suggests that the nanofiber morphology is preserved at higher temperatures. While the hexagonal packing can be observed up to 40 °C, the network is actually stable up to 70 °C and can re-form the hexagonal crystal packing with the same spacing upon cooling. Qualitatively similar behavior was observed for sample concentrations down to 4 mM. Optical microscopy at elevated temperature does not show any birefringence (see Figure S8).

To understand if intermolecular interactions were responsible for the changing line charge density with temperature, we conducted variable-temperature ^{1}H NMR spectroscopy of amphiphile **1** in D_2O (see Figure 3b). Up to 45 °C, the ^{1}H NMR spectrum shows only weak and very broad peaks, as expected for a highly aggregated system. From 50 to 90 °C, the proton resonances become sharper and more intense, suggesting that the molecules have more degrees of freedom within nanofiber. A similar transition temperature is observed by variable-temperature absorbance spectroscopy (see Figure S9). At higher temperatures, the lower packing density of the molecules results in a decrease of the filament line charge density. Therefore, the repulsion between the filaments in the network is weakened, and the nanofibers can come closer as suggested by the SAXS data.

The effects of solution concentration and temperature are summarized in Figure 4. When the solution concentration is

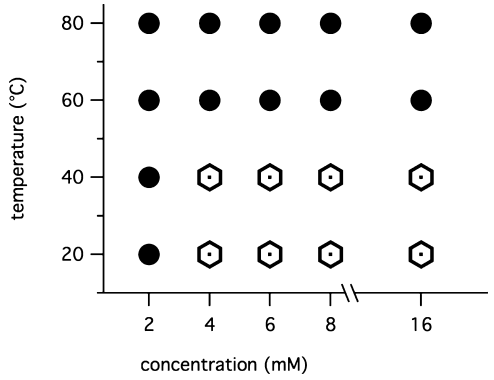

Figure 4. SAXS-determined phase diagram showing the hexagonal (open hexagons) and liquid-like ordering (filled circles) of nanofibers formed by amphiphile **1** as a function of temperature and concentration.

equal to (see Figure S10) or greater than 4 mM and the temperature of the system is below the transition temperature of 50 °C observed by ^{1}H NMR and UV–vis, the highly charged nanofibers organize into a hexagonal lattice. In this regime, the nearest-neighbor distance between these nanofibers increases as the solution is diluted. When the solution is heated above the melting temperature or diluted to 2 mM, only short-range correlations are observed between nanofibers by SAXS. For the 2 mM sample, the transition temperature is below the melting temperature of molecule **1**. Therefore, the collapse of the hexagonal packing is due to dilution of the nanofibers rather than changes on the molecular level within the nanofibers. It is likely that at this diluted concentration, the electrostatic repulsion between the charged fibers is barely sufficient to maintain the crystal structure within the confinement volume. Therefore, fluctuations of the fibers even at room temperature

dx.doi.org/10.1021/ja5082519 | J. Am. Chem. Soc. 2014, 136, 14377–14380

make the crystal unstable. In contrast, at high concentration, the loss of crystalline ordering upon heating is connected to decreased linear charge density caused by molecular level changes within the nanofiber.

CONCLUSIONS

We have reported the crystallization of highly charged cationic supramolecular nanofibers into a hexagonally packed lattice with remarkably large interfiber spacings, more than 11 times the fiber diameter. The high charge density required for this packing distance is made possible by close association of molecules within the nanofiber and the permanent +1 charge on each amphiphile. The strong electrostatic repulsions between molecules in the fibers can be counterbalanced by strong intermolecular attractions among aromatic groups and hydrophobic tails in the covalent structure of molecules. The packing structure and distance between the nanofibers can be controlled by either temperature or concentration. The dimensions of these crystalline lattices of supramolecular filaments could allow the templated growth of hybrid organic−inorganic hybrid materials on the appropriate length scale to separate excitons for energy applications.[24,25]

ASSOCIATED CONTENT

Supporting Information

Detailed synthesis, spectroscopic characterization, and X-ray scattering curves. This material is available free of charge via the Internet at http://pubs.acs.org.

AUTHOR INFORMATION

Corresponding Authors

bedzyk@northwestern.edu
s-stupp@northwestern.edu

Author Contributions

⊥These authors contributed equally.

Notes

The authors declare no competing financial interest.

ACKNOWLEDGMENTS

Materials design and synthesis was supported by the Non-equilibrium Energy Research Center (NERC) at Northwestern University, funded by the US Department of Energy (DOE), Office of Basic Energy Sciences under award no. DE-SC0000989. Characterization was supported by the U.S. Department of Energy, Office of Basic Energy Sciences under award no. (DE-FG02-00ER45810). The X-ray scattering experiments and analysis were supported by DOE-BES DE-FG02-08ER46539. S.K. was funded by AFOSR (FA9550-11-1-0275). SAXS experiments were performed at the DuPont-Northwestern-Dow Collaborative Access Team (DND-CAT) located at Sector 5 of the Advanced Photon Source (APS). DND-CAT is supported by E.I. DuPont de Nemours & Co., The Dow Chemical Company, and Northwestern University. Use of the APS, an Office of Science User Facility operated for the U.S. Department of Energy (DOE) Office of Science by Argonne National Laboratory, was supported by the U.S. DOE under contract no. DE-AC02-06CH11357. This work made use of the Biological Imaging Facility (TEM) and the Keck Biophysics Facility (optical spectroscopy). This work also relied on NMR and mass spectrometry instrumentations in the Integrated Molecular Structure Education and Research Center (IMSERC) which were funded by the NSF (NSF CHE-1048773), the International Institute for Nanotechnology (IIN) and Northwestern University. The authors thank S. Weigand for assistance with the X-ray scattering, M. Seniw for graphical assistance, M. McClendon for help with rheology, R. Korkosz in the Kanatzidis group for help with the gas pycnometer, and J. Boekhoven, J. Ortony and Y. Velichko for helpful discussions.

REFERENCES

(1) Needleman, D. J.; Ojeda-Lopez, M. A.; Raviv, U.; Miller, H. P.; Wilson, L.; Safinya, C. R. *Proc. Natl. Acad. Sci. U.S.A.* **2004**, *101*, 16099.
(2) Wang, N.; Butler, J. P.; Ingber, D. E. *Science* **1993**, *260*, 1124.
(3) Palmer, L. C.; Stupp, S. I. *Acc. Chem. Res.* **2008**, *41*, 1674.
(4) Zhang, S. M.; Greenfield, M. A.; Mata, A.; Palmer, L. C.; Bitton, R.; Mantei, J. R.; Aparicio, C.; Olvera de la Cruz, M.; Stupp, S. I. *Nat. Mater.* **2010**, *9*, 594.
(5) Berns, E. J.; Sur, S.; Pan, L.; Goldberger, J. E.; Suresh, S.; Zhang, S.; Kessler, J. A.; Stupp, S. I. *Biomaterials* **2014**, *35*, 185.
(6) Dang, X.; Yi, H.; Ham, M.-H.; Qi, J.; Yun, D. S.; Ladewski, R.; Strano, M. S.; Hammond, P. T.; Belcher, A. M. *Nat. Nanotechnol.* **2011**, *6*, 377.
(7) Aida, T.; Meijer, E. W.; Stupp, S. I. *Science* **2012**, *335*, 813.
(8) Parsegian, V. A.; Brenner, S. L. *Nature* **1976**, *259*, 632.
(9) Li, T.; Winans, R. E.; Lee, B. *Langmuir* **2011**, *27*, 10929.
(10) Li, T.; Zan, X. J.; Winans, R. E.; Wang, Q.; Lee, B. *Angew. Chem., Int. Ed.* **2013**, *52*, 6638.
(11) Valéry, C.; Paternostre, M.; Robert, B.; Gulik-Krzywicki, T.; Narayanan, T.; Dedieu, J.-C.; Keller, G.; Torres, M.-L.; Cherif-Cheikh, R.; Calvo, P.; Artzner, F. *Proc. Natl. Acad. Sci. U.S.A.* **2003**, *100*, 10258.
(12) Oosawa, F. *Biopolymers* **1968**, *6*, 1633.
(13) Safinya, C. R.; Li, Y. *Science* **2010**, *327*, 529.
(14) Solis, F. J.; Olvera de La Cruz, M. *Phys. Rev. E* **1999**, *60*, 4496.
(15) Cui, H.; Pashuck, E. T.; Velichko, Y. S.; Weigand, S. J.; Cheetham, A. G.; Newcomb, C. J.; Stupp, S. I. *Science* **2010**, *327*, 555.
(16) Yao, Z. W.; Olvera de la Cruz, M. *Phys. Rev. E* **2013**, *87*, 042605.
(17) Kunitake, T.; Okahata, Y.; Shimomura, M.; Yasunami, S.; Takarabe, K. *J. Am. Chem. Soc.* **1981**, *103*, 5401.
(18) Ikeda, T.; Tsutsumi, O. *Science* **1995**, *268*, 1873.
(19) Svergun, D. I.; Koch, M. H. J. *Rep. Prog. Phys.* **2003**, *66*, 1735.
(20) Maier, E.; Krause, R.; Deggelmann, M.; Hagenbuchle, M.; Weber, R.; Fraden, S. *Macromolecules* **1992**, *25*, 1125.
(21) Ermolina, I.; Morgan, H.; Green, N. G.; Milner, J. J.; Feldman, Y. *Biochim. Biophys. Acta, Gen. Subj.* **2003**, *1622*, 57.
(22) Gelbart, W.; Bruinsma, R.; Pincus, P.; Parsegian, V. *Phys. Today* **2000**, *53*, 38.
(23) Spaar, A.; Salditt, T. *Biophys. J.* **2003**, *85*, 1576.
(24) Sofos, M.; Stone, D. A.; Goswami, D. K.; Okasinski, J. S.; Jin, H.; Bedzyk, M. J.; Stupp, S. I. *J. Phys. Chem. C* **2008**, *112*, 2881.
(25) Briseno, A. L.; Holcombe, T. W.; Boukai, A. I.; Garnett, E. C.; Shelton, S. W.; Fréchet, J. J. M.; Yang, P. *Nano Lett.* **2010**, *10*, 334.